In vivo cancer diagnosis with optical spectroscopy and acoustically induced blood stasis using a murine MCa35 model

Brian A. Winey
Department of Physics and Astronomy, University of Rochester, Rochester, New York

Vladimir Misic
Department of Radiation Oncology, University of Rochester, Rochester, New York

Lydia Liao
Department of Imaging Sciences, University of Rochester, Rochester, New York

Kevin Parker
School of Engineering and Applied Science, University of Rochester, Rochester, New York

Bruce M. Fenton and Yan Yu[a)]
Department of Radiation Oncology, University of Rochester, Rochester, New York

(Received 28 September 2005; revised 22 March 2006; accepted for publication 24 March 2006; published 11 May 2006)

Ultrasound-induced blood stasis has been observed for more than 30 years. Most of the literature has been focused on the health risks associated with this phenomenon and methods employed to prevent stasis from occurring during ultrasound imaging. To date, experimental observations have been either *in vitro* or invasive. The current work demonstrates ultrasound-induced blood stasis in murine normal leg muscle versus tumor-bearing legs, observed through noninvasive measurements of optical spectroscopy, and discusses possible diagnostic uses for this previously undesirable effect of ultrasound. We demonstrate that, using optical spectroscopy, effects of ultrasound can be used to differentiate tumor from normal leg muscle tissue in mice. Finally, we propose a novel diagnostic algorithm that quantitatively differentiates tumor from nontumor with maximum specificity 0.83, maximum sensitivity 0.79, and area under receiver-operating-characteristics curve 0.90. © *2006 American Association of Physicists in Medicine*. [DOI: 10.1118/1.2198196]

I. INTRODUCTION

Stationary sound waves have long been known to create banding effects when solid particles are suspended in liquids; sand in air (in a cylinder), bubbles in water, etc. In 1971, Dyson *et al.* reported that stationary ultrasound waves can create bands of red blood cells *in vivo*, using chick embryos removed from the egg shell but kept alive in saline solution.[1] Later, ter Haar and Wyard reported that the banding was due to the standing pressure wave created by the ultrasound.[2] Nyborg demonstrated that even a traveling pressure wave, with small amounts of reflection at the tissue boundaries can cause banding of blood cells in the plasma medium.[3] Many have continued to study the diagnostic limits and dangers of ultrasound and ultrasound-induced stasis,[4–7] but to the best of our knowledge, no one has investigated the diagnostic potential.

A limiting factor in studying this ultrasound-induced phenomenon has been the difficulty of measuring the blood flow alterations. Previous works have required the blood vessels to be exteriorised from the abdomen of mice[5] or the removal of chick embryos from their shells[1] so as to be seen with microscopes and stereoscopes. The phenomenon has only been observed invasively and only in a few vessels immediately on the tissue surface or in vessels separated from the surrounding tissue. Methods have been suggested to avoid prolonged blood stasis during diagnostic imaging[4] and ultrasound intensity limits have been established to avoid tissue damage and to allow the blood flow to rebound.

It has been shown that oxy and deoxyhemoglobin have signature absorption and scattering effects visible in steady-state broadband diffuse reflectance optical spectroscopy.[8] Furthermore, oxyhemoglobin saturation can be determined using spectroscopic measurements of light reflected from tissue and analyzed with the diffusion approximation or the higher order P_3 approximation.[9,10] Spectral analysis performed with a P_3 approximation fit has been shown to be sensitive to dynamic changes in hemoglobin oxygen saturation due to changes in oxygen content of air inhaled by mice.[11]

Cells require a constant supply of oxygen for metabolic processes. Normally, as the cells consume oxygen, hemoglobin molecules in the blood continually replenish the oxygen supply as the blood flows through the vessels. When standing wave ultrasound is used to slow or stop the blood flow, the oxyhemoglobin saturation decreases as the available oxygen is depleted. When the blood flow is stopped or slowed for short periods of time, the oxyhemoglobin saturation can be observed to decrease, using optical spectroscopy measurements, and return to preultrasound levels shortly after the ultrasound radiation is stopped.

The current experiments combine focused standing wave ultrasound-induced blood stasis and optical spectroscopy to develop a noninvasive imaging tool with potential use in tissue diagnostics. In this paper we demonstrate that optical spectroscopy measurements of ultrasound-induced blood stasis can be used to qualify tissue type noninvasively.

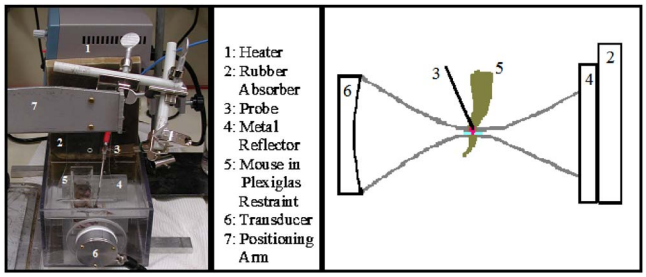

FIG. 1. Experimental setup, with the mouse leg located in the focal region of the ultrasound.

II. METHODS

A. Experiment setup

Ultrasound was generated by a 1 MHz piezoelectric ceramic crystal (Channel Industries) mounted behind a concave aluminum lens with a focal length of 7 cm. At 1 MHz the −6 dB focal zone diameter was 3 mm and the focal zone length was 30 mm. The ultrasound signal was created by a function generator (Agilent 33250A) and amplified by a rf amplifier (Amplifier Research 25A250A), monitored and recorded by an oscilloscope (Tektronix TDS 2022). The ultrasonic field was measured and characterized using a hydrophone (Onda Co. HNR 500) with spatial sensitivity of 0.5 mm. The hydrophone was calibrated with a steel ball radiometer.[12] The intensity of the ultrasound was maintained at spatial peak temporal average intensity (I_{SPTA}) $\approx 0.7\ W/cm^2$, averaged over the pulse sequence and summed over two oppositely traveling acoustic waves. The current experiments were conducted within the Food and Drug Administration (FDA) diagnostic ultrasound limits ($I_{SPTA}=0.720\ W/cm^2$) and blood stasis and banding have been observed to be reversible under these conditions.

All experiments were conducted in a Plexiglas water tank. Distilled water was autoclaved for 45 min to remove ions and microbubbles in order to prevent cavitation and scattering of the acoustic field. A 2.5 cm thick piece of aluminum was used for the acoustic reflector and a 2.5 cm thick rubber block was placed behind the aluminum to absorb any spurious acoustic energy, energy scattered by the tissue water boundary and in the side lobes of the imperfect focused ultrasound field. During experiments the water was heated to 37 °C using a circulating water heater and the rubber block was positioned to shield the data collection area from most of the water currents since moving water can interfere with spectroscopy measurements (Fig. 1).

Diffuse reflectance spectra were collected with a single 600 μm fiber, numerical aperture (N.A.)=0.22, residing at the center of a seven 600 μm fiber probe (Ocean Optics, R600-7-VIS/NIR). The center collection fiber was connected to a 2048 pixel room temperature spectrometer (Ocean Optics, USB 2000-VIS/NIR) fitted with a grating for spectrum analysis between 200 and 1100 nm. The outer six fibers were connected to a broadband halogen light source (Ocean Optics, HL 2000). The source detector separation was 1 mm, resulting in a semidonut inspection volume of $\approx 6\ mm^3$, directly under the probe and mostly within 1 mm of the tissue surface.

B. Experimental procedure

Six to eight week old C3H/Hej mice were inoculated intramuscularly to the right thigh with 10^6 MCa-35 mammary carcinoma cells, with the left hind leg muscle tissue used as control for the diagnostic portion of this experiment. To demonstrate the absence of experimental artifacts, the right leg muscle tissue was used as control and the left thigh was inoculated in two mice. To avoid scattering of the acoustic field, hair was removed from the hind legs using a depilatory agent (Nair ®) one day prior to the experiment.

The mice were sedated using a Ketamine (60 mg/kg) Xylazine (4 mg/kg) mixture injected intraperitoneally and placed in a Plexiglas restraint which positioned the leg to be examined away from the body. The probe was then fixed on the skin of the mouse leg using a positioning arm, ensuring contact but without skin compression. During data collection, the probe was held stationary, maintaining a constant pressure on the mouse skin. Optical spectroscopy measurements of hemoglobin *in vivo* are highly dependent upon surface pressure since any changes will affect the blood/hemoglobin volumes.

Once a baseline spectrum was achieved (≈4 min), the mouse and probe were moved such that the focus of the ultrasound was ≈2 mm directly under the location of the optical probe. The direction of propagation of the ultrasound and light were kept orthogonal so that the metallic probe did not enter the focus of the ultrasound and obstruct or scatter the standing acoustic wave. Also, this increased the probability of intersecting the acoustic focal region with the volume of optical inspection.

During each experiment, ultrasound was administered in 5 s bursts, with 55 second relaxation periods between bursts and a total of six bursts per leg per experimental collection. For each mouse, both legs, one with a tumor (diameter ≈ 10 mm) and one without, were subjected to ultrasound and optical spectroscopy to compare the effects in tumor versus normal leg muscle tissue. The order of inspection of the legs was altered to diminish the possibility that the results were influenced by the depth of the anesthesia, which can directly affect the blood velocity.

Ultrasound pulse information for each experiment was monitored and collected with the oscilloscope and stored for later signal correlation studies. Optical spectra were collected with the supplied Ocean Optics software at 500 ms intervals in order to increase the signal-to-noise ratio (SNR) by reducing the appearance of unwanted higher frequency signal fluctuations and quantum noise.

The raw optical spectra were corrected for the curvature of the light source intensity, which was a function of wavelength specific to the halogen source. The intensity curve of the light source was obtained using a diffuse reflectance standard. The optical signal then was cropped to avoid the spectral regions of low light levels (<400 nm) and regions near

the end of the spectrometer's sensitivity (>1000 nm), regions where noise is especially high. Ultimately, the spectra were cropped to regions between 475 and 650 nm where significant optical absorption occurs due to oxy/deoxyhemoglobin presence, especially in short (≈1 mm) source detector separation configurations, and few other absorbers (i.e., water) exert significant effects.

The spectra were analyzed using a P_3 approximation method detailed in Refs. 10 and 11 to gather oxy/deoxyhemoglobin concentrations, as well as scattering information, before, during, and after ultrasound pulses.

In addition to the P_3 fitting algorithm, several isolated wavelengths were initially considered (515, 528, 540, 560, 579, and 578 nm), due to the characteristic effects of oxy/deoxyhemoglobin shifts at these points, but ultimately the ratio of intensities (I) at two wavelengths, 560 and 540 nm, was chosen. The ratio of I_{560}/I_{540} was observed to be significantly affected by the presence (or absence) of the ultrasound. The intensities at 560 and 540 nm are dependent upon the oxy/deoxyhemoglobin saturations, at 560 (540) nm the reflected signal increases (decreases) as the oxyhemoglobin concentration increases.

C. Immunohistochemistry and image analysis of vascular spacing and area

To visualize blood vessels open to flow, an intravenous (i.v.) injected stain $DiOC_7$ was injected one minute prior to tumor freezing, which preferentially stains cells immediately adjacent to the vessels.[13] Tumor and muscle sections were imaged using a 20× objective, digitized, background-corrected, and analyzed using Image-Pro software.[13] Color images were acquired and digitally combined under two staining conditions. First, images of the $DiOC_7$ were obtained immediately after cryostat sectioning. Following staining, the sections were returned to the same stage coordinates, and antipanendothelial antigen (Pharmingen, San Diego, CA) images were acquired to mark total anatomical vessel locations. Vessels were quantified using automated image analysis techniques.[14] Briefly, distance map filters converted pixel intensities of the vessel images to intensity levels proportional to the distances between tumor cells and the nearest vessels. This distance map was multiplied by an image of white grid points on a black background to obtain a spatial sampling of the distance map intensities, which are proportional to the distances to the nearest vessel (vessel spacing).

D. Signal/ultrasound correlation

A computer algorithm was written to speed the data analysis. In order to demonstrate the effects of the ultrasound on the optical signal, a correlation model was adapted. Using the stored ultrasound pulse data, the algorithm calculated the degree of correlation with the I_{560}/I_{540} data.

Correlation between the I_{560}/I_{540} ratio and ultrasound bursts was visually evident in most normal leg muscle tissue samples. The bursts of ultrasound caused pronounced drops in the observed I_{560}/I_{540} signals. This correlation was quantified and demonstrated to be significantly different for probe readings of tumor versus normal leg muscle tissue responses. The algorithm used in this experiment was as follows:

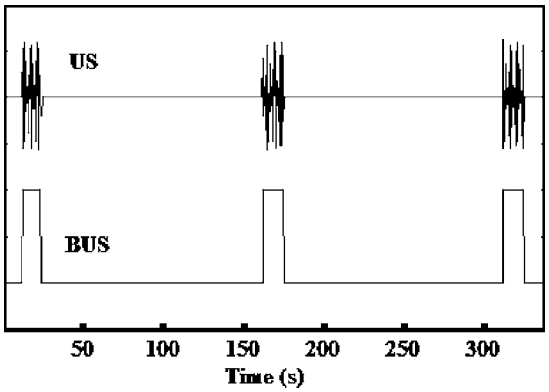

FIG. 2. Illustration of a typical ultrasound pulse sequence (US) and its corresponding "boxed" representation (BUS).

1. The original ultrasound (US) signal was modified ("boxed") (Fig. 2.) as

$$\mathrm{BUS} = \begin{cases} 0, & \text{US off} \\ 1, & \text{US on} \end{cases}. \tag{1}$$

2. The general slope (i.e., trend) of the I_{560}/I_{540} signal was approximated using a second degree polynomial interpolation, and the BUS (1) was scaled down and adjusted to the signal trend:

$$\mathrm{AUS} = \mathrm{trend} - \mathrm{BUS}/20. \tag{2}$$

3. To characterize the I_{560}/I_{540} versus US correlation, we used cross covariance of I_{560}/I_{540} and AUS. Cross covariance assesses the degree to which two variables covary or vary together. It is computed as the mean of the products of the mean deviations for each variable in the observed set. Thus, the cross covariance between recorded I_{560}/I_{540} signal (R) and adjusted (AUS) ultrasound signal was calculated as the cross-correlation function of two sequences with their means removed, which by definition is given by

$$X\mathrm{Cov}(m) = E_n\{[R(n+m) - \mathrm{MR}]^* \mathrm{conj}[\mathrm{AUS}(n) - \mathrm{MAUS}]\}, \tag{3}$$

where MR and MAUS stand for the means of R and AUS, respectively, E stands for the mathematical expectation, conj is the complex-conjugate operator, and m and n are position indices in the signal. The complex conjugate operation is included in the definition even though [AUS(n)-MAUS] is a real quantity.

4. The XCov signal was smoothed using the Savitzky-Golay (polynomial) smoothing filter, with the polynomial order 3 and window size 41.[15]
5. The standard deviation of the smoothed XCov signal was calculated.

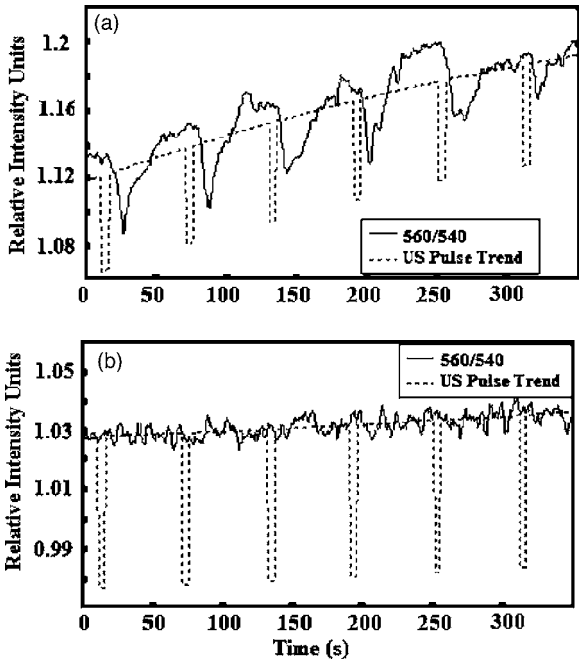

FIG. 3. The ratio I_{560}/I_{540} signal with the trend modulated ultrasound pulse signal superimposed for a typical (a) normal leg muscle tissue and (b) tumor tissue. Notice the much larger ultrasound induced contrast in the normal leg muscle signal.

6. Steps 1–5 were performed for both tumor and normal leg muscle tissue samples, and the ratio of the measurements

$$\mathrm{Std}(X\mathrm{Cov}_{\mathrm{nontumor}})/\mathrm{Std}(X\mathrm{Cov}_{\mathrm{tumor}}) \quad (4)$$

was calculated and recorded.
7. Steps 1–6 were repeated for a total of 24 mice.

E. Diagnostic algorithm

Upon confirmation of a stronger correlation between ultrasound bursts and changes ("dips") in the observed signal for the normal leg muscle tissue compared with the tumor tissue (Fig. 3), we constructed a novel diagnostic algorithm that utilized that information.

1. The ultrasound (US) signal was modified as in Eq. (1).
2. Locations of the centers of each ultrasound burst were found and used to split I_{560}/I_{540} to nonoverlapping "windows" bounded by those centers. The end of observation at the right side bounded the rightmost "window" (Fig. 4.).
3. The general slope (i.e., trend) of the I_{560}/I_{540} signal was approximated using second degree polynomial interpolation, and the difference between trend and $I_{560/540}$ was calculated.
4. The positions of the local minima of the difference function (calculated for each "window") were calculated.
5. A new signal (comb) consisting of ones at the positions of local minimums, and zeros elsewhere was constructed (Fig. 4.).

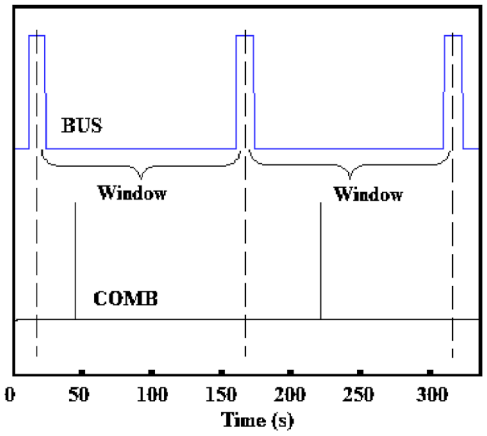

FIG. 4. Illustration of "boxed" ultrasound signal (BUS), observation "windows," and comb signal with spikes at the positions of local minima (calculated for each "window").

6. The maximum of the correlation between the ultrasound (BUS) signal and comb signals was calculated.
7. The ratio

$$r = [\mathrm{sum}(\mathrm{comb}) - \max(\mathrm{corr})]/\mathrm{sum}(\mathrm{comb}) \quad (5)$$

was calculated and compared to a decision threshold dt.

The experiment was repeated for varying values of the decision threshold, and a receiver-operating characteristics (ROC) curve was calculated.

III. RESULTS

A. Tests of the experimental setup

Initial tests of our ultrasound setup included a repeat of Dyson's seminal experiment, but with lower acoustic intensities [$(\mathrm{SPTA}) = 0.7\ \mathrm{W/cm^2}$] and lower frequencies ($f \approx 1$ MHz). The ultrasound was observed visually to stop blood flow in the chick embryo vessels, causing bands to form for short periods of time (data not shown).

In order to perform a noninvasive test regarding the efficacy of the ultrasound in the mouse leg, a laser Doppler system (Transonic BLF21) was used to verify blood flow slowing or stasis due to ultrasound in the healthy leg muscle and the tumor tissue. This technique relies on the interference between a light-emitting diode (LED) signal beam and the reflected beam, revealing the velocity profiles of the reflecting objects visualized as sidebands to the original beam. For the laser Doppler technique, a baseline velocity measurement was achieved after three minutes in the healthy muscle tissue. This was required since the tissue needed to equilibrate to the presence of the fiber probe on the surface of the skin. The measurements of the tumor tissue, however, never achieved a stable baseline and the velocity was chaotic.

From the laser Doppler measurements, it was clear that in a small target volume of healthy tissue the average velocity of the blood was slowing during the ultrasound pulse [Fig. 5(a)], but there was no noticeable effect in the tumor tissue [Fig. 5(b)]. The vertical lines denote when the ultrasound

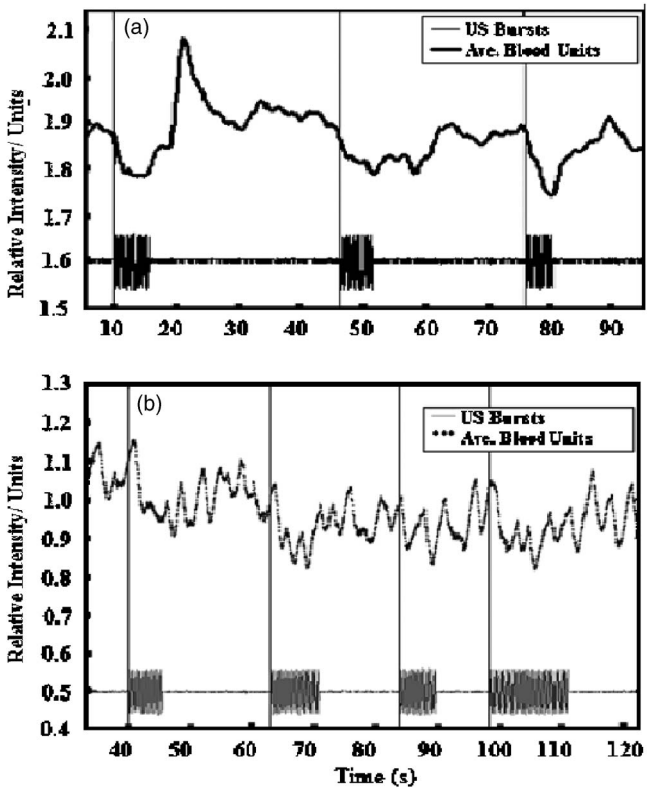

FIG. 5. Laser Doppler relative average volume velocity shown with ultrasound bursts and vertical lines for reference for normal leg muscle (a) and tumor (b) tissue samples. The normal leg muscle samples have greater blood volume flow rates.

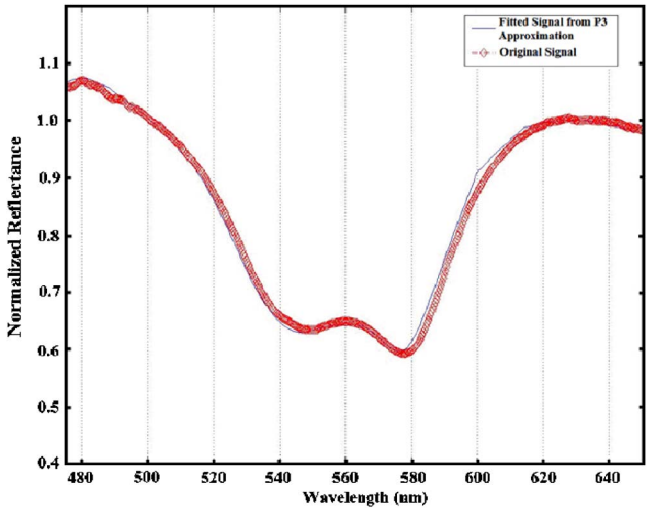

FIG. 6. A sample of an *in vivo* spectra of a healthy tissue sample with a P_3 fit used to determine the oxy/deoxyhemoglobin saturations and the scattering properties of the tissue.

was introduced, with the ultrasound being turned off after 5 s. The large velocity peak in Fig. 5(a) following the tissue recovery after the first pulse is believed to be due to vessel dilation as the tissue responded to the oxygen deprivation, or post-ischemic reactive hyperemia. The peak was not observed after subsequent pulses. It is believed that the tissue was oxygen enriched following the vessel dilation and was not given enough time to return to relaxed oxygen levels. This was taken into consideration for the optical spectroscopy experiments and the ultrasound pulses were delivered after longer delays.

The laser Doppler technique can only measure an average change in velocity because it incorporates the Doppler shift from all moving reflecting particles in a tissue sample. Since the ultrasound induced stasis will depend upon the vessel orientation relative to the ultrasound direction of propagation, blood flow in vessels aligned with the ultrasound will be stopped and blood flow in vessels perpendicular to the ultrasound will continue to flow, thus decreasing the net effect on the average flow observed by the laser Doppler.

The laser Doppler probe had a maximum observation depth of $\approx$1 mm and a volume of inspection of $\approx$1 mm^3. When this same volume element was inspected with white light in the presence of ultrasound, there were measurable changes in the oxyhemoglobin saturation.

Before every experiment, the presence of standing wave ultrasound was visually confirmed using an interference technique. The density bands formed by standing wave ultrasound create an interference pattern when light passes through the tank. The location and intensity of the focal zone were also confirmed using the hydrophone between experiments.

B. *In vivo* diffuse reflectance optical spectroscopy

Typical reflectance spectra obtained *in vivo* from the healthy tissue sample are shown in Fig. 6. Complete spectra data (400–1100 nm) were stored for every experimental collection period ($\approx$10 min/leg) at 500 ms intervals and then cropped as previously described.

The cropped spectra were analyzed with a technique similar to the one described by Finlay and Foster, which is applicable for small source detector separations.[11] The P_3 fitting algorithm assumes that in a specific wavelength range (380–750 nm) the absorption spectrum is dominated by a linear combination of the absorption spectra of oxy- and deoxyhemoglobin. This can be expressed as

$$\mu_a(\lambda) = \mathbf{a}_1 \mu_{a\mathrm{HbO}}(\lambda) + \mathbf{a}_2 \mu_{a\mathrm{Hb}}(\lambda), \tag{6}$$

where $\mu_{a\mathrm{HbO}}(\lambda)$ and $\mu_{a\mathrm{Hb}}(\lambda)$ are the millimolar absorption coefficients of oxy- and deoxyhemoglobin at wavelength λ, and $\mathbf{a}_1$ and $\mathbf{a}_2$ are their concentrations, respectively. The absorption spectra were taken from data compiled by Prahl. [16]

The scattering spectrum were assumed to be of the form

$$\mu_s' = \mathbf{a}_3 \lambda^{-\mathbf{a}_4}, \tag{7}$$

where $\mathbf{a}_3$ is the scattering coefficient and $\mathbf{a}_4$ the scattering exponent, which, for a tissue sample, is approximately 1. The *in vivo* spectra were fit using a MATLAB supplied routine,"lsqcurvefit," which uses a least squares fitting algorithm given some initial vector $\mathbf{a}$ and Eqs. (6) and (7). The spectra were normalized prior to fitting. The algorithm was placed inside another program written to randomly select vector $\mathbf{a}$ within some predetermined limits and continue this process

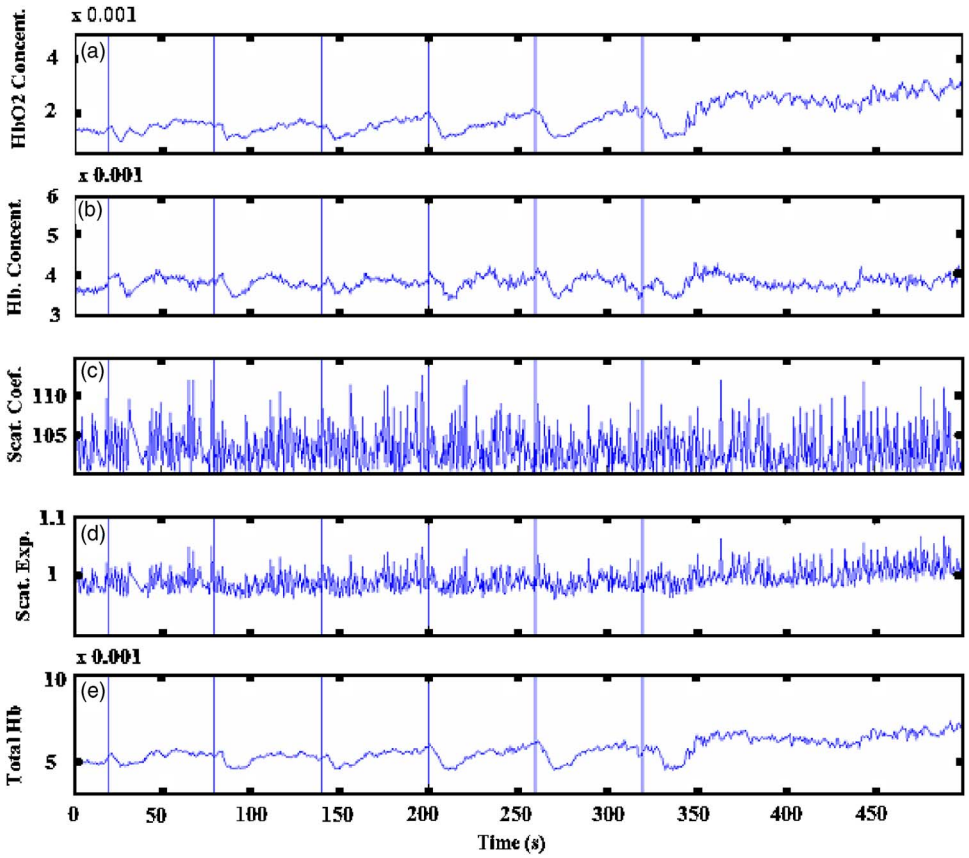

FIG. 7. Parameters derived using the P_3 fitting algorithm applied to the collected broadband diffuse reflectance spectra: (a) oxyhemoglobin concentration; (b) deoxyhemoglobin concentration; (c) scattering coefficient; (d) scattering exponent; and (e) total hemoglobin concentration. The vertical lines reference the beginning of the five second bursts of ultrasound.

with the condition that the sum of the residues was minimized and that the χ^2 function approached 1.

Results of the fitting process for one spectra of one healthy mouse leg are presented in Fig. 6. The hemoglobin concentrations ($\mathbf{a}_1$ and $\mathbf{a}_2$), the scattering parameters ($\mathbf{a}_3$ and $\mathbf{a}_4$), and the total hemoglobin concentrations for one spectrum are given in Fig. 7. The I_{560}/I_{540} ratio signal is shown in Fig. 8. It can be shown, using the P_3 fitting algorithm, that the ratio I_{560}/I_{540} correlates to oxyhemoglobin concentrations and that the ultrasound has no observable effect on the scattering properties of the tissue in the wavelength range considered.

The results displayed a large drop in oxyhemoglobin concentration when ultrasound is introduced. The deoxyhemoglobin, however, also displayed a drop in concentration. The drop was less significant and as a portion of the total hemoglobin, it actually increased. This seems to imply that the oxyhemoglobin was not only decreasing due to consumption without replenishing but also due to a decrease in blood volume. This might be due to a squeezing of tissue due to the presence of the acoustic standing wave.

The calculation of these results from a complete experimental collection period required 13 hours of CPU time. While the minimum residue search program was not maximized for efficiency and was programmed in MATLAB, known to be much slower than programs running in C, the entire P_3 fitting process was less than ideal for our experiments and for the immediate generation of diagnostic information in a clinical setting.

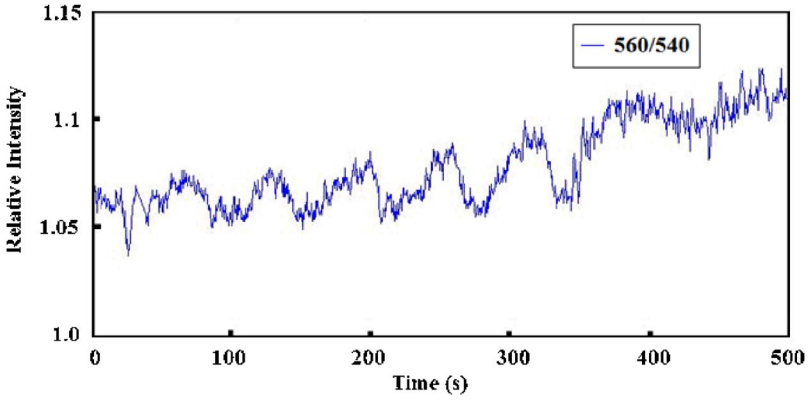

FIG. 8. The $I_{560/540}$ signal which reflects the changes in oxyhemoglobin concentrations.

In order to estimate more efficiently changes in tissue oxygenation, a technique known as oximetry was employed. Oximetry is a technique that uses a ratio of intensities at two or more wavelengths to measure tissue properties. Various commercial products use oximetry to measure blood properties, e.g, hemoglobin saturation. Oximetry is generally insensitive to many physiological artifacts, such as scattering properties and blood volume, and, without calibration, is incapable of determining absolute oxy/deoxyhemoglobin concentrations. Oximetry was used because of its speed and ease of calculation and because it was observed to reflect the oxyhemoglobin dynamic changes.

C. Correlation studies

By visual comparison of the I_{560}/I_{540} signal with the ultrasound signal, one can generally establish temporal correlation between these two signals in the normal leg muscle scans and the absence of correlation in the tumor scans [Figs. 3(a) and 3(b)]. The drops in the I_{560}/I_{540} ratio signal have been consistently observed in normal leg muscle scans and are mostly absent in tumor scans. The slope trend observed in Fig. 3(a) was not consistently observed and is believed to be a second order ultrasound effect, possibly due to the acoustic pressure affecting the vessel diameter or the global vascular response to the rise in deoxyhemoglobin. It was observed that the mathematical correlation between the ratio signal and the ultrasound signal in general was significantly higher in normal leg muscle cases, than in tumor cases (Fig. 9).

To demonstrate that it was possible to establish the mathematical correlation between the I_{560}/I_{540} signal and the ultrasound signal, a simple computer algorithm was written. The standard deviation of the cross covariance of the ultrasound square pulse (Fig. 2) and the I_{560}/I_{540} signal were computed in order to provide a quick estimate of the degree of correlation. Repeatable large decreases in the oxyhemoglobin and the I_{560}/I_{540} signal corresponding to the timing of the ultrasound pulses produce the greatest degree of correlation. The standard deviation of the cross covariance was chosen instead of the maximum because a maximum can be misleading if there is a random alignment of peaks in the signals whereas the standard deviation is more telling of trends and the consistent matching of peaks. Also, the trend of the I_{560}/I_{540} signal was subtracted from the ultrasound pulse data in order to decrease the effects of signal slope on the cross covariance.

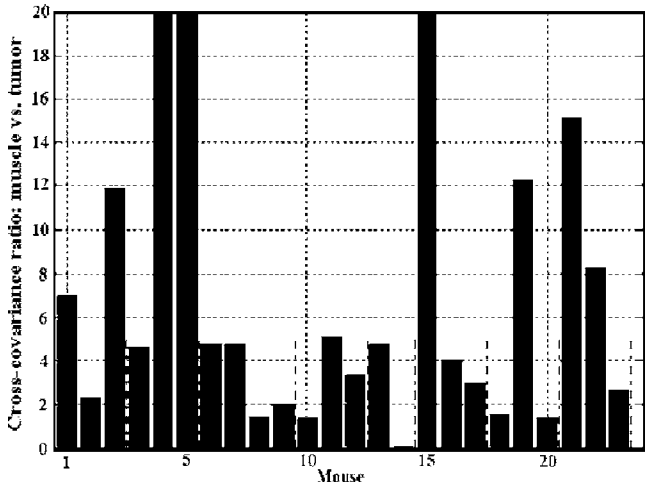

FIG. 9. The I_{560}/I_{540} signal in normal leg muscle tissue is better correlated to the ultrasound than the same signal for tumor tissue, measured for the same mouse to compensate for physiological differences in mice population.

The standard deviation of the cross covariance for each leg, tumor, and normal leg muscle, and for each mouse, was calculated and compared to the opposite leg of the same mouse as a ratio [Eq. (4)]. The ratios for 24 mice are presented in Fig. 9. The strength of the correlation is reflected in the height of the bar in Fig. 9. The ratio of the standard deviations [Eq. (4)] was greater than 1 (one) in all but one experiment, and greater than 2 (two) in 75% of measured

TABLE I. Experimental data used to calculate ROC.

Thold	tp	fn	tn	Tp	Sens.	Spec.	PPV	NPV
0.00	1.00	0.00	0.29	0.71	1.00	0.29	0.59	1.00
0.10	1.00	0.00	0.29	0.71	1.00	0.29	0.59	1.00
0.20	0.92	0.08	0.58	0.42	0.92	0.58	0.69	0.88
0.30	0.92	0.08	0.58	0.42	0.92	0.58	0.69	0.88
0.35	0.83	0.17	0.75	0.25	0.83	0.75	0.77	0.82
0.40	0.79	0.21	0.83	0.17	0.79	0.83	0.83	0.80
0.45	0.79	0.21	0.83	0.17	0.79	0.83	0.83	0.80
0.50	0.58	0.42	1.00	0.00	0.58	1.00	1.00	0.71
0.60	0.54	0.46	1.00	0.00	0.54	1.00	1.00	0.69
0.70	0.04	0.96	1.00	0.00	0.04	1.00	1.00	0.51
0.80	0.00	1.00	1.00	0.00	0.00	1.00	nd	0.50
0.90	0.00	1.00	1.00	0.00	0.00	1.00	nd	0.50
1.00	0.00	1.00	1.00	0.00	0.00	1.00	nd	0.50

True positives (tp) are correctly identified tumor tissue samples, and true negatives (tn) are correctly identified normal leg muscle tissue samples.

mice. Having a ratio greater than one means that the I_{560}/I_{540} signal of the normal leg muscle tissue is more correlated to the ultrasound signal than the I_{560}/I_{540} signal of the tumor tissue. In other words, a ratio greater than one means that the "dips" in the I_{560}/I_{540} signal of the normal leg muscle sample are deeper than the "dips" in the tumor sample.

After demonstrating a large degree of correlation between the I_{560}/I_{540} signal and the ultrasound pulse signal for normal leg muscle tissue samples, a second computer algorithm was written with the aim of creating a diagnostic program based on an *in vivo* experimental observation. The diagnostic algorithm divided the I_{560}/I_{540} signal into windows corresponding to the spacing of ultrasound bursts in the ultrasound signal. Within each window, local minima were located and coded as ones, while the remainder of the signal was coded as zeros. If the local minima were consistently and regularly spaced, they were assumed to correspond to the ultrasound-induced "dips" in the I_{560}/I_{540} signal. If the ultrasound had a small effect on the I_{560}/I_{540} signal, the local minima would not be consistently or regularly spaced.

The cross covariance of this new binary signal and the ultrasound square pulse signal was calculated to measure the degree of consistency and regularity of the local minima. The maximum of the cross-covariance signal was normalized to the number of ultrasound pulses gathered from the pulse signal and subtracted from one, generating a value between 0 and 1 [Eq. (5)]. A smaller value ($r \approx 0$) denoted a strong degree of correlation between the local minima and the ultrasound pulse signal, meaning that the local minima consistently occurred at time intervals corresponding to the ultrasound bursts. A larger value ($r \approx 1$) denoted a weak degree of correlation and local minima appearing at irregular and inconsistent times with respect to the ultrasound burst.

The diagnostic algorithm applied a decision threshold to determine which measurements were gathered from tumor or normal leg muscle tissue samples.[17] If the value or r was greater than the threshold, the sample was classified as a tumor. The algorithm achieved the best results with the decision threshold 0.40; specificity was 83.3% and sensitivity was 79.2%. Complete results of this experiment are presented in Table I with the ROC given in Fig. 10.

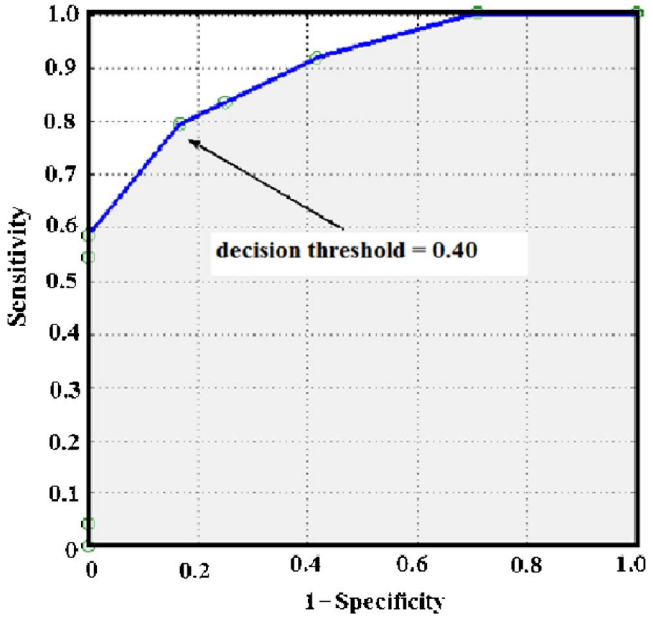

FIG. 10. ROC curve for the diagnostic algorithm. Decision threshold varied from 0.1 to 1 in 0.05 steps. Area under the curve is 0.90.

The hypothesis of this experiment is that there are physiological and rheologic differences between healthy tissue and tumor tissue that could cause the tissues to respond differently to the presence of standing wave ultrasound. To study the physiological differences, immunohistochemical studies were conducted on the tumor and normal leg muscle tissue samples following imaging and cryostat sectioning.

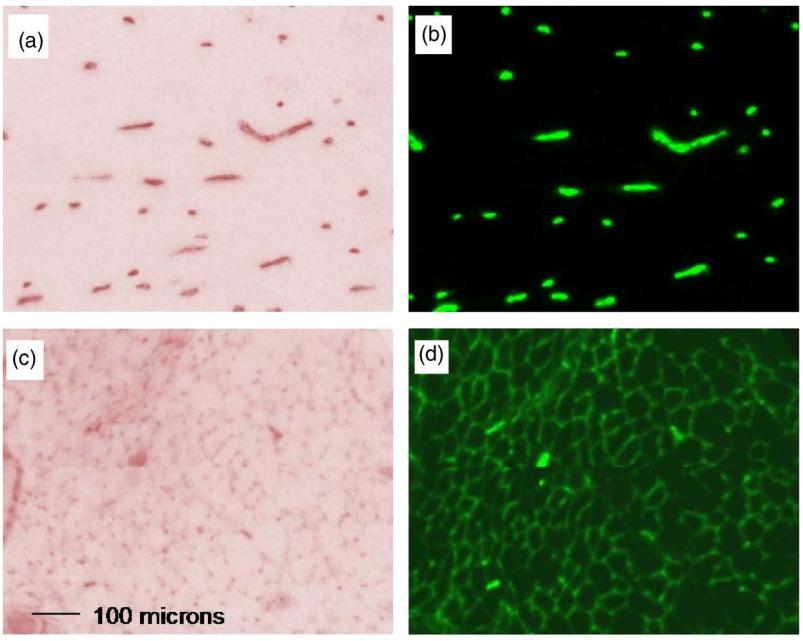

FIG. 11. Vessel staining of (a) tumor and (c) normal leg muscle tissue samples. Corresponding perfused vessel stains for the same samples are shown in (b) and (d), respectively.

TABLE II. Immunohistochemistry results.

Mouse number		Median vessel spacing (μm)	Percent vessel area (%)	Median perfused vessel spacing (μm)	Percent perfused vessel area (%)
Tumor					
	15	25.00	4.00	37.49	1.94
	16	25.00	4.88	68.74	1.12
	17	27.08	4.25	34.37	4.07
	18	29.16	3.34	49.99	1.10
	19	22.91	4.69	31.25	3.13
	20	20.83	6.01	58.32	1.63
	21	25.00	5.14	49.99	1.69
	22	29.16	4.51	43.74	1.66
	23	33.33	4.21	45.83	2.16
	24	25.00	4.74	43.74	1.71
	25	35.41	3.55	49.99	1.67
	26	29.16	4.41	68.74	1.33
	27	22.91	4.11	43.74	1.42
	28	22.91	4.60	39.58	2.04
	29	18.75	5.65	31.25	2.40
	30	27.08	4.32	39.58	2.75
	31	20.83	5.16	33.33	2.33
	35	22.91	5.32	58.32	1.15
	36	20.83	3.97	35.41	1.72
	37	22.91	4.85	45.83	1.62
Average		25.31	4.59	45.46	1.93
STD		4.29	0.67	11.22	0.73
Nontumor					
	16	8.33	16.21	12.50	8.98
	17	8.33	17.48	12.50	7.61
	18	6.25	19.68	14.58	6.03
	19	10.42	16.76	10.42	18.54
	20	10.42	15.23	25.00	2.67
	21	10.42	14.85	12.50	9.94
	22	10.42	15.59	12.50	4.36
	23	12.50	12.82	14.58	8.99
Average		9.63	16.08	14.32	8.39
STD		1.91	2.02	4.51	4.80

Figure 11 illustrates total and perfused vessels in both tissue types following i.v. injection of a fluorescent perfusion marker ($DiOC_7$). From these images, total and perfused blood vessel area and spacing of the vessels were determined (Table II). The immunohistochemistry data in Table II demonstrates that tumors increased spacing of both total and perfused vessels (signifying reduced vascular densities) as well as a reduction in total and perfused vascular area (which indicates a decrease in overall blood volume).

IV. DISCUSSION

While the I_{SPTA} was maintained below the FDA limit for diagnostic ultrasound, the I_{SPTP} (spatial peak, temporal peak intensity) of the acoustic standing wave achieved levels ($\sim$2.4 W/cm^2) that can cause tissue heating during prolonged exposure. Since the traveling wave was reflected upon itself, the measured traveling wave intensities, I_{SPTA} and I_{SPTP}, do not accurately measure the intensity of the stationary acoustic field. The standing wave is a superposition of two acoustic waves, traveling in opposite directions, one having an initial I_{SPTA} of 0.50 W/cm^2 (I_{SPTP}=1.91 W/cm^2) and the other having an initial I_{SPTA} of approximately 0.32 W/cm^2 (I_{SPTP}=1.19 W/cm^2) after being attenuated during the first pass through the leg of the mouse, assuming an attenuation coefficient of muscle tissue[18] and perfect coupling between the tissue and the water bath. The average total I_{SPTA} in the focal zone was 0.66 W/cm^2 (I_{SPTP} =2.4 W/cm^2) due to attenuation of the two traveling waves.

The soft tissue thermal index (TIS) of this stationary acoustic field was not exceedingly high during insonication. The maximum TIS was 4.3 and the maximum temperature increase was less than 1 °C (ΔT=+0.91 °C) in the focal region for brief periods of time (seconds) after the five second acoustic pulse, which is within tissue damage threshold. The mechanical index (MI) was very low, with a maximum value of 0.5. All of these values were calculated using the equations provided in Ref. 18, with the equation specific intensities and pressures.

Although the ultrasound intensities employed have been shown to create very little heating of the tissue and have not been observed in cryostat sectioning to damage tissue, the effects of ultrasound on vessel diameter have yet to be addressed, i.e., does standing wave ultrasound constrict or dilate the vessels? High intensity traveling ultrasound waves have been shown by Dalecki *et al.* to exert pressure on the walls of frog heart cavities.[19] The pressures required to cause banding in moving blood are much lower than the intensities needed to deform the tissue of the heart but some tissue deformation might occur.

As predicted from prior studies,[1,2] the presence of the standing wave ultrasound caused changes in the blood velocity [Fig. 5(a)], and, consequently, changes in the oxyhemoglobin concentrations. The processes involved in acoustically induced blood stasis are neither simple nor straightforward and many physiological questions remain unanswered concerning the ultrasound-induced effects.

Previous papers (e.g., Ref. 20) have shown almost invariably that transplanted murine tumor models have reduced oxygen saturations when compared to surrounding normal tissue. This reduction of oxygen saturation is due primarily to insufficiencies of the tumor vasculature to adequately supply oxygen. It was our hypothesis that, due to the tumor tissue tendency to have less blood, fewer vessels, and less oxygen saturation, the tumor will not have a large response to standing wave ultrasound when measured with optical spectroscopy. In tumors, the baseline of the I_{560}/I_{540} tended to be much lower and the oxyhemoglobin concentration measured with the P_3 algorithm tended to be lower than the normal leg muscle tissue samples.

Initial tumor and normal leg muscle tissue oxyhemoglobin concentrations varied from mouse to mouse, possibly due to the depth of the anesthesia. Some mice with higher initial oxyhemoglobin concentrations demonstrated ultrasound-induced contrast in the tumor tissue. This contrast however

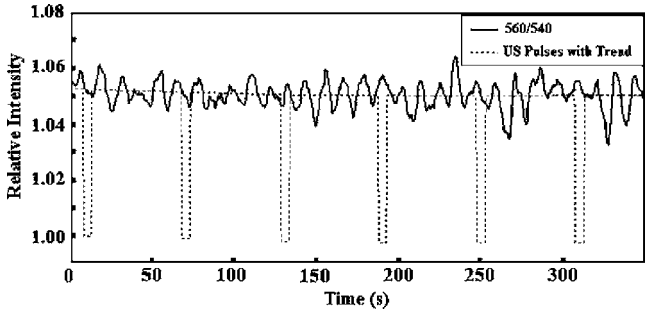

FIG. 12. The I_{560}/I_{540} ratio signal for nontumor tissue with the trend modulated ultrasound pulse superimposed. The ultrasound-induced drops are difficult to distinguish.

was generally less substantial than the contrast observed in the normal leg muscle tissue of the same mouse. Comparison of the ultrasound-induced contrast of each leg to the opposite leg of the same mouse was implemented to reduce the mouse to mouse variance of oxyhemoglobin saturation. As noted in Ref. 11, there are potentially large differences in the diffuse reflectance spectra gathered from different mice and from various locations of a single tumor in each mouse.

For each mouse, the difference in ultrasound-induced oxyhemoglobin concentration changes between tumor and normal leg muscle tissue could result from differences in blood vessel counts and blood oxygen saturation. When these tumors were analyzed with laser Doppler, the ultrasound-induced stasis appeared to have little effect on the Doppler measurement, possibly due to the multidirectional and interwoven mesh of blood vessels, somewhat in contrast to the more orderly flow of skeletal vessels. In addition, the tumors generally had lower initial oxyhemoglobin saturations than the corresponding normal muscle tissue of the opposite leg.

In general, the ultrasound-induced contrast was much more pronounced when initial hemoglobin concentrations were elevated in both tissue samples. This elevation could be due to inflammation of the skin, abrasion, higher vessel counts, large vessels in close proximity to the probe, less pressure exerted by the probe on the skin, etc. Although, experimental procedures were designed to decrease the effects of inflammation, abrasion, and probe force on the skin, it was unclear whether such factors led to the varying spectral responses between mice. Additional studies are needed to further investigate these factors.

Decreases in the observed I_{560}/I_{540} ratios were predictable and generally corresponded to the ultrasound bursts, but were not always easily observable (Fig. 12). In some experiments it was hard to distinguish between responses of tumor and normal leg muscle tissue. If the probe was positioned in the proximity of a major blood vessel in the tumor, the observed signal behaved in a manner similar to the normal leg muscle cases (i.e., substantial decreases in the signal were correlated to the ultrasound bursts). Also, the relatively small size of the tumors made experiments sensitive to the probe positioning with respect to the surface vessels and the position of the ultrasound.

For clinical application and for larger organs or animal models, the experimental apparatus must be altered. The single focused transducer in line with a metal reflector will only work for exteriorized tissue samples or easily accessible *in vivo* tissue samples, i.e, breast tissue and muscle tissue. To compensate for more difficult tissue locations, a dual in-phase focused transducer system can be used, where the overlapping focused fields will produce a stationary acoustic field. Wu *et al.* have demonstrated stationary wave production for large tissue phantom using two ultrasound sources.[21] Focused ultrasound is known to diverge in tissue, causing the focal zones to enlarge. This would limit the spatial sensitivity of the ultrasound induced stasis.

Diffuse optical spectroscopy is limited by absorption and probe geometry. Using techniques of optical coherence tomography (OCT), whole-breast imaging is possible. [22] Light in the near infrared (NIR) can travel several centimeters before absorption and source detector separations of several centimeters can probe depths of several centimeters. Also, catheter optical probes can be placed on the surface of less accessible tissue samples, i.e., prostates. While both stationary acoustic fields and diffuse optical spectroscopy are complicated in larger tissue models, it is possible to construct an apparatus capable of inspecting the effects of acoustically induced blood stasis in larger tissue samples. Work is underway in our laboratory to design and build one such system for human breast cancer characterization.

V. CONCLUSION

The current study demonstrates that there are substantial and predictable ultrasound-induced changes in the I_{560}/I_{540} ratio signal obtained through *in vivo* spectroscopic measurements of diffuse light reflected from tumor and normal leg muscle mouse tissue. The ratio signal was shown to be better correlated to the ultrasound signal for normal leg muscle tissue than tumor tissue. Using a simple diagnostic algorithm, it was shown that the area under the ROC curve achieved a value of 0.90, for a threshold value of 0.45 with a specificity of 0.83 and a sensitivity of 0.79. The methodology of infrared spectroscopy with ultrasound-induced contrast appears highly promising for noninvasive tissue typing, where normal and malignant tissues tend to contain different vascular environments.

ACKNOWLEDGMENTS

This work was supported by the U.S. National Institutes of Health Grant No. CA107860 awarded by the National Cancer Institute.

[a]Electronic mail: yan_yu@urmc.rochester.edu

[1]M. Dyson, B. Woodward, and J. B. Pond, "The flow of red blood cells stopped by ultrasound," Nature (London) **232**, 572–573 (1971).
[2]G. ter Haar and S. J. Wyard, "Blood cell banding in ultrasonic standing wave fields: a physical analysis," Ultrasound Med. Biol. **4**, 111–123 (1978).
[3]W. L. Nyborg, "Microsonation of cells under near-threshold conditions," *Proc. 2nd World Congress of Ultrasonics Med.* (American Elsevier, New York, 1974), pp. 360–366.

[4]G. ter Haar and M. Dyson, "Effects of ultrasound on circulation," Biorheology **4**, 207 (1977).
[5]G. ter Haar, M. Dyson, and S. P. Smith, "Ultrastructural changes in the mouse uterus brought about by ultrasonic irradiation at therapeutic intensities in standing wave fields," Ultrasound Med. Biol. **5**, 167–179 (1979).
[6]B. S. Brown, "How safe is diagnostic ultrasonography," Can. Med. Assoc. J. **131**, 307–311 (1984).
[7]W. L. Nyborg, "Biological effects of ultrasound: development of safety guidelines. Part II: General Review," Ultrasound Med. Biol. **27**, 301–333 (2001).
[8]W. G. Zijlstra, A. Buursma, and W. P. Meeuwsen-van der Roest, "Absorption spectra of human fetal and adult oxyhemoglobin de-oxyhemoglobin, carboxyhemoglobin and methemoglobin," Clin. Chem. **37**, 1633–1638 (1991).
[9]T. J. Farrell, M. S. Patterson, and B. C. Wilson, "A diffusion theory model of spatially resolved, steady-state diffuse reflectance for the noninvasive determination of tissue optical properties *in vivo*," Med. Phys. **19**, 879–888 (1992).
[10]E. L. Hull and T. H. Foster, "Steady-state reflectance spectroscopy in the P_3 approximation," J. Opt. Soc. Am. A **18**, 584–599 (2001).
[11]J. C. Finlay and T. H. Foster, "Hemoglobin oxygen saturations in phantoms and *in vivo* from measurements of steady-state diffuse reflectance at a single, short source-detector separation," Med. Phys. **31**, 1949–1959 (2004).
[12]F. Dunn, A. J. Averbuch, and W. D. O'Brien, Jr., "A primary method for determination of ultrasonic intensity with an elastic sphere radiometer." Acoustica **38**, 58–61 (1977).
[13]B. M. Fenton, S. F. Paoni, J. Lee, C. J. Koch, and E. M. Lord, "Quantification of tumor vascular development and hypoxia by immunohistochemical staining and HbO_2 saturation measurements," Br. J. Cancer **79**, 464–471 (1999).
[14]B. M. Fenton, S. F. Paoni, B. K. Beauchamp, and I. Ding, "Zonal image analysis of tumour vascular perfusion, hypoxia, and necrosis," Br. J. Cancer **86**, 1831–1836 (2002).
[15]S. J. Orfanidis, *Introduction to Signal Processing* (Prentice-Hall, Englewood Cliffs, NJ, 1996).
[16]S. A. Prahl "Optical properties of hemoglobin," http://omlc.ogi.edu/spectra/hemoglobin/summary.html (1999).
[17]D. L. Sackett, R. B. Haynes, P. Tugwell, and G. H. Guyatt, *Clinical Epidemiology: A Basic Science for Clinical Medicine* (Lippincott Williams and Wilkins, Baltimore, 1996).
[18]W. R. Hendricks, D. L. Hykes, and D. E. Starchman, *Ultrasound Physics and Instrumentation* (Mosby, New York, 1995).
[19]D. Dalecki, C. H. Raeman, S. Z. Child, and E. L. Cartensen, "Effects of pulsed ultrasound on the frog heart. 3. The radiation force mechanism," Ultrasound Med. Biol. **23**, 275–285 (1997).
[20]B. M. Fenton, S. F. Paoni, B. G. Grimwood, and I. Ding, "Disparate effects of endostatin on tumor vascular perfusion and hypoxia in two murine mammary carcinomas," Int. J. Radiat. Oncol., Biol., Phys. **57**, 1038–1046 (2003).
[21]Z. Wu, L. S. Taylor, D. Rubens, and K. J. Parker, "Shear wave focusing for three-dimensional sonoelastography," J. Acoust. Soc. Am. **111**, 439–446 (2002).
[22]W. Luo, F. T. Nguyen, A. M. Zysk, T. S. Ralston, J. Brockenbrough, D. L. Marks, A. L. Oldenburg, and S. A. Boppart, "Optical biopsy of lymph node morphology using optical coherence tomography," Technol. Cancer Res. Treat. **4**, 539–548 (2005).